ECN Spray D visualization of the spray interaction with a transparent wall under engine-like conditions. Part I: Non-reactive impinging spray.

Jesús E. Peraza[a], F.J. Salvador[b], Jaime Gimeno[b,*], Santiago Ruiz[b]

[a] *FEV Iberia SL, World Trade Center Barcelona, 08039 Barcelona, Spain.*
[b] *CMT - Motores Térmicos, Universitat Politècnica de València, 46022, Valencia, Spain.*

*Corresponding author. E-mail address: jaigigar@mot.upv.es.

Abstract

The possibility for a jet of fuel to collide against the surfaces of the combustion chamber or the piston bowl into a thermal engine, has a direct effect on the droplets breakup and the spray atomization. In order to study the spray/wall interaction phenomenon and its influence on the macroscopic spray behavior, a diesel spray was visualized when impinging on a flat wall made of quartz at various ambient, injection and wall position conditions. Two high-speed cameras were employed simultaneously to perform Schlieren imaging and diffuse back illumination diagnostics, in order to observe both spray vapor and liquid phases during their contact with the wall. The experiments were performed in a constant pressure-flow test rig, able to reproduce diesel-like thermodynamic conditions. Two different fuels (n-dodecane and diesel #2) were injected within the chamber by employing a single-hole injector referred to as Spray D into the framework of ECN research group. To place the wall in the spray path, a wall positioning structure capable of being fitted into the chamber and of support the wall at various inclination angles and distances from the injector tip, was designed. The test rig was filled with N_2 to keep an inert atmosphere and isolate the spray development from possible alterations produced by combustion. Results provide the influence of the injected fuel, operating and wall conditions on the macroscopic features of the transient spray in terms of spreading onto the wall and spray thickness characterized both temporally and spatially. Spray spreading was evaluated by a novel penetration-based parameter. It showed to be proportional to the square root of time similarly as free-penetration and is largely affected by the wall inclination respect to the spray axis. Spray angle showed to be influenced by the morphology of the spray that affects its air entrainment capacity and that changes with a wall respect to a free-jet configuration. This variation in the morphology also has a remarkable effect on spray evaporation, characterized in terms of liquid length and liquid spreading onto the wall. Finally, the large amount of data was used to obtain correlations for all the studied parameters.

Keywords: Spray-wall interaction, Fuel jet impact, Post-impingement characteristics, Schlieren imaging, Diffuse back illumination, Engine Combustion Network

1. Introduction

The experimental study of fuel injection and spray development should faithfully represent the actual processes that occurs within the cylinder of an internal combustion engine (ICE). A large number of experimental researches have been carried out in the last years trying to achieve more realistic conditions in order to provide a reliable source of data for CFD codes validation and tuning [1–3]. However, a process that occurs irremediably in small-bore diesel and directed injection gasoline engines, and that is not commonly considered in injection-combustion analysis is the spray-wall interaction (SWI). The influence of the jet impact against the piston walls on combustion is very complex. On the one hand, the jet-wall interaction may improve the air-fuel mixing, by generating secondary atomization and enhancing the gas entrainment into the spray. Nevertheless, a fuel film can be formed on the walls after the impingement, rising the formation of soot and unburned hydrocarbons, besides a reduction of the engine efficiency produced by a worsening in the combustion and the heat transfer from the reactive spray to the walls [4–6].

Cite as:
Peraza, J.E., Salvador, F.J., Gimeno, J., Ruiz, S., "ECN Spray D visualization of the spray interaction with a transparent wall under engine-like conditions. Part I: Non-reactive impinging spray", *Fuel* (2022), Vol. 307, 121699, doi: https://doi.org/10.1016/j.fuel.2021.121699

Nomenclature

Acronyms	
ASOE	After start of energizing
ASOI	After start of injection
CMOS	Complementary metal-oxide-semiconductor
CPF	Constant-pressure flow (facility)
DBI	Diffused backlight illumination
D2	Diesel #2 (abbr. used in plot legends)
ECN	Engine Combustion Network
EGR	Exhaust gases recirculation
LED	Light-emitting diode
k-factor	Conicity factor used in industry
LED	Light-emitting diode
nC12	n-Dodecane (abbr. used in plot legends)
SWI	Spray-wall interaction

Variables	
C	Coefficients of discharge (defined by subscript)
D	Diameter
d	Distance
k-*factor*	Conicity factor used in industry
LL	Liquid length
$\dot{M}$	Spray momentum
p	Pressure
R	*R-parameter*
Re	Reynolds number
S	Penetration
T	Temperature
Y	Spray spreading
Z	Spray thickness or height

Greek Symbols	
Δp	$p_{rail} - p_{amb}$
ϕ	Spray angle
ρ	Density
τ	Start of SWI
θ	Angle (of the wall)

Subscripts	
$+$	Wall upwards direction
$_{100}$	Total distillation (temperature)
$_{a}$	Area (coefficient)
$_{amb}$	Ambient condition
$_{l}$	Liquid phase
$_{o}$	Nozzle outlet
$_{rail}$	In-rail, of injection (pressure)
$_{thXX}$	Measuring point location (in mm)
$_{w}$	Related to the wall

Some experimental researches have been proposed to characterize the spray-wall interaction phenomenon, being possible to divide them into two main categories similar to what is stated by several authors [7, 8]: The study of the impact of single drops, and the analysis of wall impingement of sprays. Although the isolated droplet impact is a simplified approach respect to the impinging spray one, the literature on the first one has contributed to the understanding of the influence of a great deal of variables on spray-wall interaction, such as the properties of the fluid and the surface and the characteristics of formation and impingement of the droplets [9, 10]. Phase-Doppler Anemometry [10, 11], MIE scattering [12, 10, 13] and Backlight Diffused Illumination (DBI) [14, 15] are some of the optical techniques employed in the diagnostics of mean drop size, Weber number and drop velocity profiles in the wall impact regions. Rioboo et al. [16] agree with Moita and Moreira [17] in how different disintegration mechanisms are promoted by the impact energy and how them are affected by fluid viscosity, drop diameter and the impact angle. Also, surface temperature measurement systems have been used to study the heat transfer between the drops and the wall and their drops regimes [12, 11, 18], obtaining correlations relative to each regime. On the other hand, experiments of sprays, which involve multiple drops interacting between them and a more real emulation of spray systems such as injectors in ICEs represent an increase in the complexity of the process. Akop et al. [19] carried out a series experiments in an environment at atmospheric pressure, taking into account the plate angle, observing that a pronounced inclination decreases the adhered fuel mass ratio. Another experiments [6, 20, 21] indicate that the spray momentum has an important effect on the spray expansion along the wall and gas entrainment. Arcoumanis and Chang [22] employed fast response thermocouples to determine that the pre-impingement spray velocities play a key role on the local heat transfer rates. Regarding the fuel film that remains on the wall after the impingement, it has been studied by techniques such as Laser-Induced Fluorescence in some works [23, 24], which concluded that the mass of the film tends to increase at lower chamber temperatures and higher injection pressures.. Zhang et. al. [25] have concluded via Schlieren imaging that under turbulent combustion conditions, the vaporization of the spray is improved due to the heat transfer effect. More realistic works with full-view transparent pistons [26] have explored different combustion strategies such as HCCI and PPC, evaluating the effect of the wall on both CO and CO_2 emissions.

There is a large number of institutions which make research on injection-combustion topics. Unfortunately, it is quite difficult to unify criteria when investigation is performed experimentally and numerically, considering the different methodologies, techniques, test rigs and CFD codes that are employed by them [27, 28]. In order to reduce the uncertainties produced by those differences, the Engine Combustion Network (ECN) was created as an open forum that promotes collaboration between research centers and pursues the generation of a high-qual-

ity and reliable shared database [29]. The group focuses efforts in the study of determined injection systems at a range of target conditions that are of significant interest for the engine research community [27, 28] (ambient nominal conditions of $900\,\mathrm{K}$ and $22.8\,\mathrm{kg\,m^{-3}}$ and n-dodecane as main mono-component fuel for research).

Spray-wall interaction is a process that is still not fully understood whose better comprehension is needed to assess a more accurate analysis of air-flow mixing and combustion processes in ICEs [30–32], specially in a world with different engine design trends such as downsizing for automotive powertrains and the increase of power density in heavy-duty hardware. This investigation is an attempt to throw light on the spray-wall interaction phenomenon under high-pressure and high-temperature conditions, similar to the reached into engines combustion chambers. The research is divided into two parts: The first of them, which is presented in this document, covers the study of the SWI at evaporative inert conditions in absence of O_2 in order to understand the fluid-dynamic behavior of the spray when it collides with a flat wall. The second part, which involves the study of combustion at reactive conditions, is described in another article [33]. A Bosch single-hole injector designed to avoid internal flow cavitation was employed to inject two different fuels into a constant-pressure flow facility (CPF) in a wide spectrum of injection diesel-like conditions. A quartz wall was placed in front of the injector at different distances from the nozzle outlet and at different inclination angles in order to deeply analyze the effect of the impingement conditions on the interaction after the impact. It required the design of a versatile system introduced into the vessel to support the wall, allowing to vary its position respect to the injector. High-speed cameras where used to observe laterally both the vapor and liquid phases of the spray through Schlieren and DBI techniques respectively. Additionally, this article serves as the first part of a whole study that covers the impinging spray combustion process in its second half.

This manuscript has been structured in four sections. First, the present introduction. Next, the experimental methods, hardware employed and the optical setups are described, including explanations of the facilities and processing methodologies. Later, results are presented and discussed. The main conclusions obtained from this work are drawn in the last section.

2. Materials and methods

2.1. Spray visualization chamber and injection system

The investigation was conducted in an optically-accessible continuous-flow constant pressure test rig that makes possible to visualize sprays at diesel-like chamber conditions. This high-pressure and high-temperature vessel (hPhTC) has three optical accesses of $128\,\mathrm{mm}$ of diameter placed orthogonally between them. In the side without any window the injector is fixed horizontally, and a continuous ethylene glycol flow is in direct contact with it in order to steadily control the injected fuel temperature by means of a cooling system detailed in [34]. The vessel has a two-layer configuration in order to keep thermal losses at the minimum and to improve the temperature homogeneity inside the inner wall, while the second one has a purely structural function. The gap between both layers is filled with insulating material.

The facility works with a controlled mixture of dry air and N_2 that allows in-chamber oxygen concentrations between 0% (for high-temperature inert research such as this part of the investigation) and 20.9%. The chemical composition of the gas in the chamber is permanently monitored by a lambda sensor [35, 36]. As shown in Figure 1, the pressurized gas is initially stored in reservoirs from a compressor, enters into the test rig through a $30\,\mathrm{kW}$ electric heaters system. After the gas exits from the vessel, it is cooled, filtered and recirculated to the compressor again or released to the atmosphere. The control system is a closed loop PID, where both the pressure in chamber and the heaters output power are controlled. This test rig is not only able to operate at conditions up to $950\,\mathrm{K}$ and $13\,\mathrm{MPa}$, but also has the capability of provide nearly quiescent and steady thermodynamic conditions, which enables continuous and repeated observation at a wide range of conditions.

An axial single-hole Bosch 3-22 injector which is one of the target hardwares of the Engine Combustion Network was employed in this campaign, specifically, the Spray D, serial number #209135 [29]. The injector has a convergent nozzle (*k-factor* of 1.5) with an outlet diameter of $190\,\mu\mathrm{m}$ and has a rounded entrance that has been manufactured in order to avoid cavitation phenomenon in the inner flow. Many geometrical features of the injector can be found on the ECN webpage [29] and it has been hydraulically characterized in previous works such as Payri et al. [37].

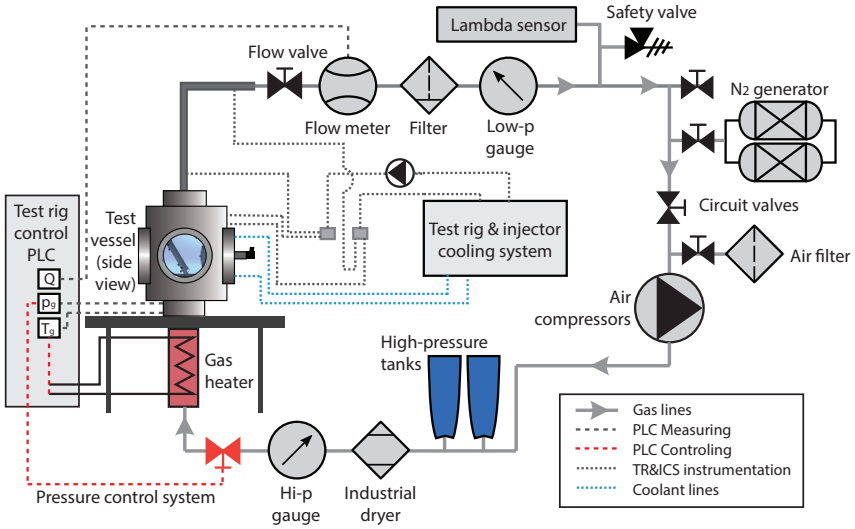

Figure 1: Lateral view of the high-pressure and high-temperature visualization vessel.

The injection setup consisted of an standard Common-Rail system, which is mainly constituted by a conventional rail with a pressure regulator and a high-pressure volumetric Bosch CP3 pump which is powered by an electric motor. The injector was kept at 363 K using an injector holder through which an ethylene glycol flow at a constant and controlled temperature runs in direct contact with the injector during all the testing time [34]. The injector was inserted in the test rig by this holder and connected to the common rail with a high pressure line.

2.2. Test matrix

Most of test conditions are of common interest into the ECN group [29], and can be found in Table 1. A wide range of operating conditions has been covered, including different high ambient temperatures and densities, injection pressures and wall positions which have been varied in terms of distance from the injector tip to the plate (d_w) and wall angle to the horizontal (θ_w). Another variation to be taken into account is the injected fuel. Two fuels have been used for the experiments and their properties are shown in Table 2. Each point has been repeated 10 cycles in order to determine the statistical accuracy of the reported averaged result.

Table 1: Test conditions summary.

Parameter	Values	Units
Fuel[a]	n-Dodecane - Diesel #2	-
Injector	Bosch 3-22 Spray D	-
Energizing time	2.5	ms
Tip temperature	363	K
Oxygen perc. (O_2%)	0 (inert conditions)	%
Gas temperature (T_{amb})[a]	700 - 800 - 900	K
Gas density (ρ_{amb})[a]	22.8 - 35	kg/m^3
Injection pressure (p_{rail})	50 - 100 - 150 - 200[b]	MPa
Wall distance (d_w)[a]	30 - 50	mm
Wall angle (θ_w)[a]	30 - 45 - 90	°

[a] Not all possible combinations of these parameters have been performed.
[b] Only for diesel tests.

Table 2: Fuel properties for n-dodecane and diesel #2 [29].

Fuel Property	n-Dodecane	Diesel	Units
T_{100}	489	623	K
Cetane number	87	46	-
Lower heat value	44.17	42.975	MJ/kg
Fuel density[a]	752.1	843	kg/m^3
Aromatics concent.	0	27	%
H_2 mass concent.	15.3	13.28	%
Kin. viscosity[b]	1.5	2.35	mm^2/s
Flash point	356	346	K
Sulfur content	0	9	ppm
Plot legend reference[c]	nC12	D2	-

[a] Value at 15 °C
[b] Value at 40 °C
[c] Name employed in plot legends due to spacing reasons

2.3. Wall supporting system

In Figure 2-left, the system that was employed to support the wall in a determined position inside the vessel is shown. This assembly was designed to ensure that the wall accomplishes with accuracy the desired conditions of inclination angle and distance from the injector tip. A protective cap is used in order to be the first layer between the hot gases and the injector body, and to support insulating material against the injector holder. Two folded sheets are screwed to it, and are used to hold two fixed 'U' shaped structures which have the function of bearing the wall assembly at the desired distance-angle configuration. Depending on this target position, a determined pair of exchangeable frames is used to support the wall holder. Those frames can be changed and come in different shapes depending on the desired configuration for the wall. The JGS1 fused quartz wall is pressed against its holder by means of four wall hooks, that are regulated with screws. Figure 2-right shows a view from the test rig window ($128\,\mathrm{mm}$ diameter), allowing a wide area to observe the interaction phenomenon between the spray and the wall ($100\,\mathrm{mm} \times 60\,\mathrm{mm}$).

2.4. Experimental techniques

2.4.1. Liquid phase visualization through DBI

DBI (Diffuse back-illumination imaging) is a technique that has been widely employed in liquid and spray diagnosis for several applications, such as droplet size distribution [38], spray liquid phase visualization [39, 40] and soot measuring [41, 42]. In this case, when employed to determine the liquid length, it consists on the consideration of the spray liquid phase as the dark silhouette of the spray when the background is illumined with a diffused light.

The setup utilized can be seen in Figure 3 where the main light trajectory represented in dashed blue arrows. The $57\,\mathrm{ns}$ pulse of light is emitted by a fast white LED and then, it passes through an engineered plane diffuser and a fresnel lens, which smooths the light intensity and homogenizes the images background. This arrange is set ensuring that the complete test area is covered. Then, the light reaches a 50-50 beam splitter that reflects perpendicularly half of it towards the test region, to finally go towards another beam splitter and which directs the beam to the high-speed camera. In the test region, the presence of fuel in liquid phase will block the light path while it would be slightly attenuated by vapor phase sprays and finally, undisturbed in the case of zones with only ambient gases. Nevertheless, the light beams are not parallel and then the attenuated (deviated rays) and the unaffected ones are not clearly distinguished. The black region in the recorded images, formed by the blocked light, is considered the liquid fuel region. Specifications about the setup can be found in Table 3.

2.4.2. Single-pass Schlieren imaging

The vapor phase of the spray has been recorded using the Schlieren imaging technique. It is sensitive to the first spatial derivative of density, so it is quite useful for the visualization of gaseous phenomena that are not visible to the naked eye. This technique is based on the use of parallel beams through an interest zone in order to observe their deflection. In this particular case, the technique is used to detect spray boundaries between

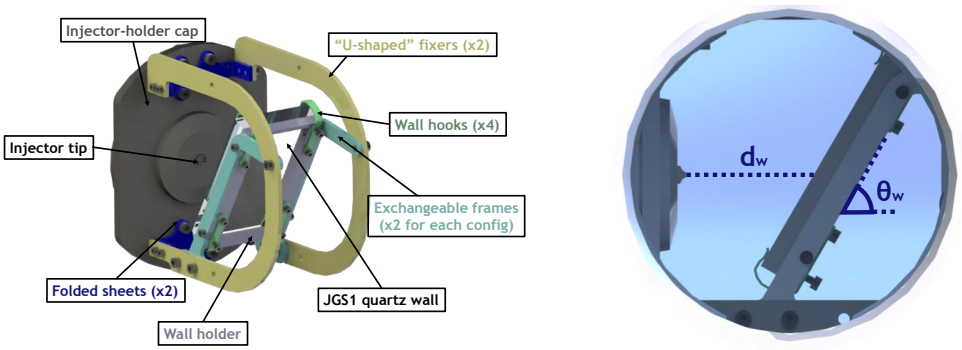

Figure 2: Wall mounting system (for a wall configuration of d_w = $50\,\mathrm{mm}$; θ_w = $60°$). Left: Assemblage indicated by pieces. Right: View from a lateral optical access of the vessel

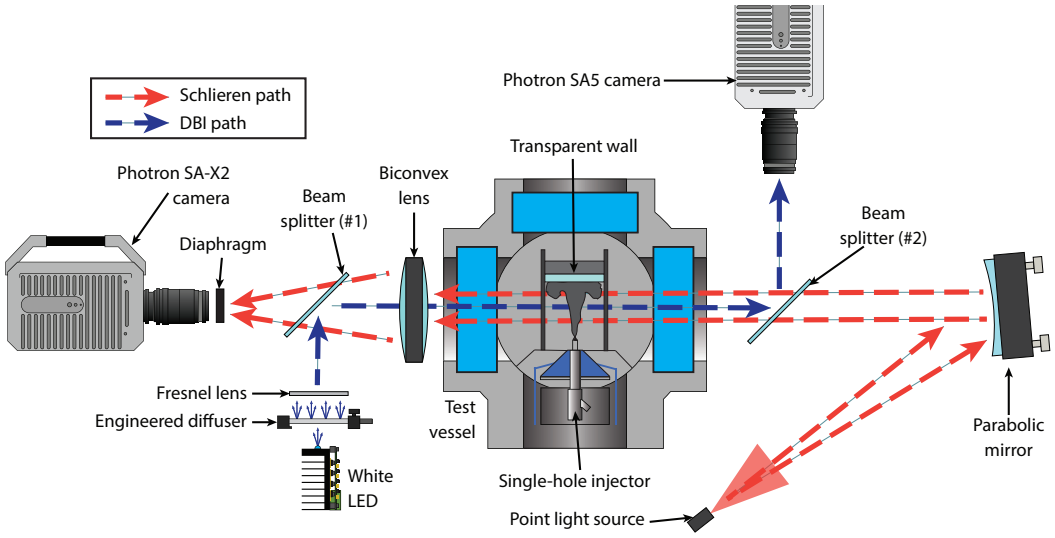

Figure 3: Optical setup employed for both liquid and vapor phases visualization. DBI light main path is indicated in blue dashed arrows, while the red one are illustrating the Schlieren beams path

the vaporized fuel of the spray and the background gases into the vessel, which is possible due to the different refraction indexes that are associated to density dissimilarities.

In red dashed arrows, Figure 3 indicates the path of the Schlieren light through the vessel and the optical material employed in this technique application. A continuous Xe-Arc lamp is connected to an optical fiber which ends in the punctual light source shown in the bottom of the scheme. The beams travel to a parabolic mirror, which has the objective to collimate the light and deviate it to the vessel. The parallel beams are differently deviated due to the density gradients inside the vessel. Then, the rays are collected by a biconvex lens, which makes them converge to the high-speed camera, where diaphragm keep back the deviated rays of enter to the camera lens. Table 3 contains more detailed information about the optical setup.

Table 3: Details of the optical setup for the employed techniques.

	Camera	Lens diameter	LED pulse duration	Diaphragm gap diam.	Frame rate	Shutter time	Px/mm ratio
Diffused back-illumination	Photron SA5	100 mm	57 ns	-	25 kfps	1.00 μs	7.00
Schlieren imaging	Photron SA-X2	100 mm	-	4 mm	40 kfps	1.01 μs	5.88

2.5. Image processing

The spray images were processed using an algorithm which has been internally developed and extensively employed [35, 43]. Regardless of the optical technique, the general processing methodology is broadly the same. However, the type of images is specified in a pre-processing step in order to adapt the strategy to the particularities of each set of images.

The background of the image is prepared to be subtracted in order to normalize its luminosity to a zero level. Images obtained with both techniques receive a different treatment. In the case of DBI images, the background is obtained as the average of the first captures before the start of injection (SOI). This is possible since the background can be considered as static during the injection event for DBI images. On the contrary, in the case of Schlieren imaging, it is necessary the calculation of a new background (a dynamic one) for each image. The calculation of that Schlieren background follows the combination of two strategies: the use of a threshold based on the pixel intensity levels of the image and the detection of pixel variations by the study of the pixel-wise standard deviation of three consecutive images. The images obtained are then filtered via morphological operations in order to prevent background irregularities. Finally, the filtered images from both processing approaches are

combined in a weighted average in order to obtain a final average image and the spray contour. Figures 4 and 5 gather different samples of the images that are obtained for both liquid and vapor phases of the spray by using the previously described optical setup and the detected contours with the processing methodology.

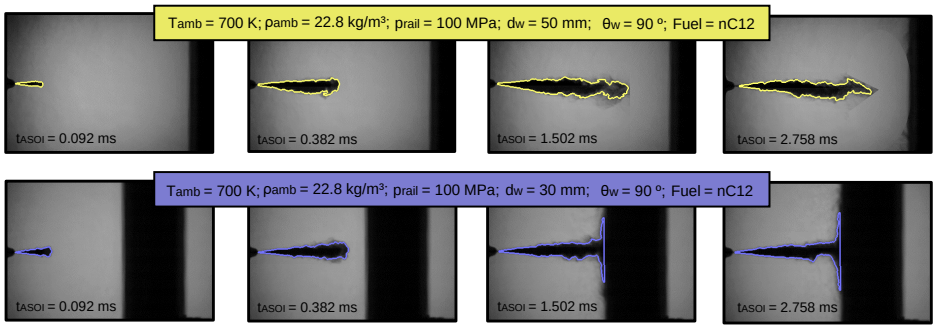

Figure 4: Samples of random reps of the images observed via DBI (T_{amb} = 700 K; ρ_{amb} = 22.8 kg m^{-3}; p_{rail} = 100 MPa; θ_w = 90°; Fuel = nC12). Top set: Wall at d_w = 50 mm. Bottom set: Wall at 30 mm from the injector tip.

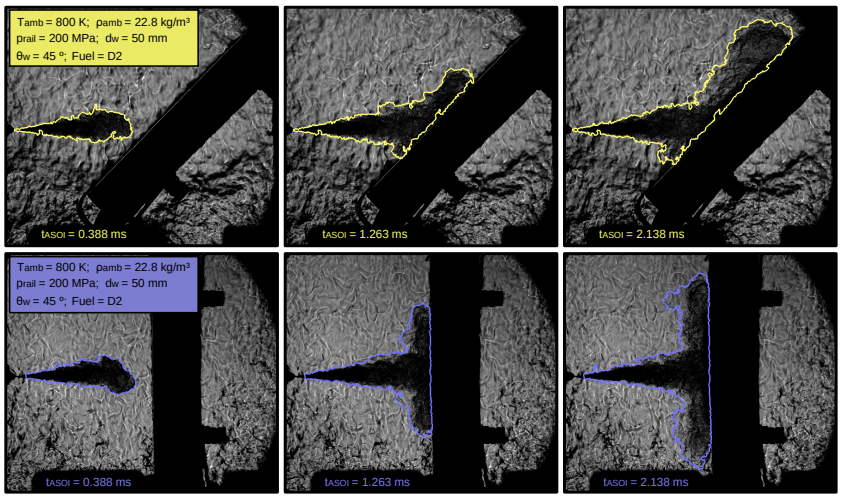

Figure 5: Samples of a random repetition of the images observed via Schlieren imaging at inert conditions (T_{amb} = 800 K; ρ_{amb} = 22.8 kg m^{-3}; p_{rail} = 200 MPa; d_w = 50 mm; Fuel = D2). Top set: Wall inclined θ_w = 45°. Bottom set: Wall angles set at θ_w = 90°

2.6. Contour analysis

Figure 6 shows two different images obtained from the Schlieren technique, where the contour obtained with the previously described approach is shown. The metrics that has been calculated from the contours vary if the contour has been taken before or after the impact. Keeping that in mind, the variables calculated for the free-jet part of the injection event are:

- **Free spray penetration (S):** is considered as the distance between the furthest point of the spray contour and the nozzle tip.
- **Spray angle (ϕ):** The spray angle is calculated as the formed between two linear fits of the spray contour as shown in Figure 6 left picture. These fits are made using a data range between the 10% and the 50% of the measured free-jet penetration.

On the other side, the variables that have been calculated after the start of SWI, are:

- **Spray spreading along the wall (Y_+):** The spray spreading along the wall is calculated as the distance between the 'collision point' and the furthest contour point in the direction towards the top of the wall. This 'collision point' is defined as the interception between the wall plane and the free-jet axis, not being necessarily the first point of the wall that enters in contact with the spray.
- **Spray thickness along the wall (Z_{th}):** Three consecutive points from the 'collision point' (indicated in dark blue crosses in Figure 6 right image) at 10 mm; 20 mm and 30 mm from it, are used to measure this variable as the maximum normal distance between the wall and the spray contour.

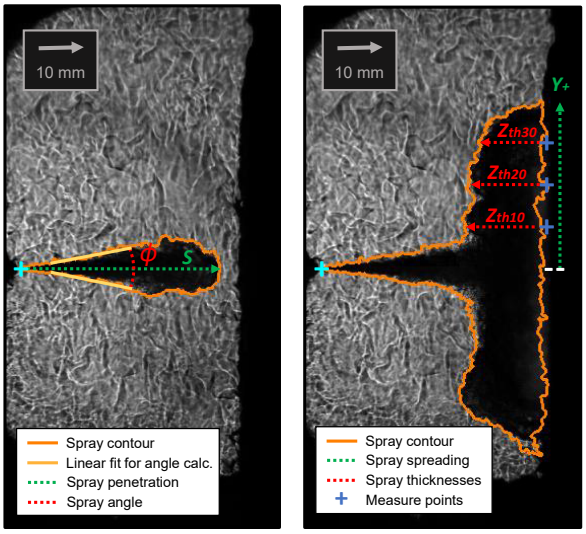

Figure 6: Macroscopic parameters calculated from the side spray images. (T_{amb} = 800 K; ρ_{amb} = 22.8 kg m^{-3}; p_{rail} = 150 MPa; d_w = 50 mm; θ_w = 90°; Fuel = nC12). Left: Free-jet (t_{ASOI} = 430 µs). Right: Spray-wall interaction (t_{ASOI} = 2110 µs).

Additionally a new metric that is defined as the derivative respect to the square root of time of both free-jet penetration and spray spreading has been defined and referred to as *R-parameter*:

- ***R-parameter* for penetration and spreading (R_S and R_Y):** In accordance with several models from spray theory [44, 45], under the assumption of a cone-shaped spray, at the steady part of its evolution it can be considered that penetration is proportional to the time rised to the power of 0.5, which makes its derivative respect to the square root of time to be a nearly constant value, as shown in the sample of Figure 7, where both penetration (left) and its derivative respect to the square root of time (right) are shown for a different ECN injector [35]. This constant parameter to study penetration has shown to be particularly useful since it can be analyzed regardless of the considered temporal reference [35, 3, 6].

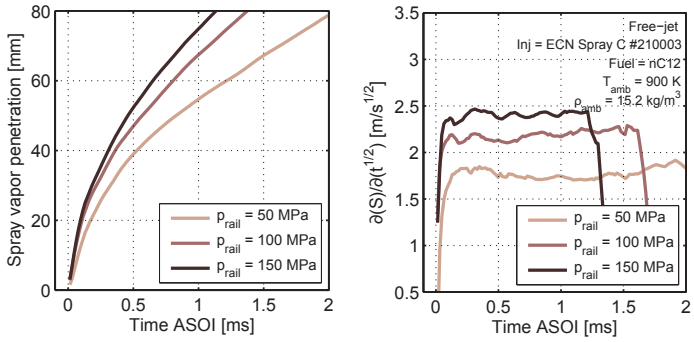

Figure 7: Sample of spray penetration and its *R-parameter* at free-jet non-reactive conditions for an ECN Spray C injector (plot adapted from [35]). Left: Vapor penetration by injection pressure. Right: *R-parameter* for same conditions.

- **Start of SWI (τ_w):** This variable is defined in this work as the time when $S_v = d_w$ (v subscript denotes vapor). Nevertheless, it could be the case that the furthest point of the spray contour detected on the spray axis becomes stagnant few millimeters before reaching the wall due to the strong density gradients produced in the background near from the wall surface that can be observed via Schlieren imaging. Considering this, a numerical gridded fit was made using the spray penetration data from $0.2 \cdot d_w$ to $0.8 \cdot d_w$ in order to avoid the transient start of the injection and the part when the spray is near to the wall. This fit is then extrapolated to d_w and the time when they match is taken as τ_w as seen in Figure 8.

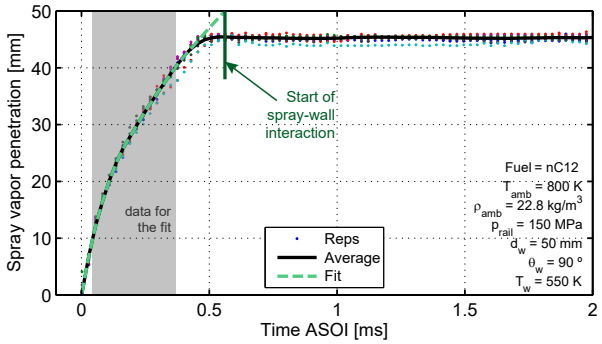

Figure 8: Calculation of start of SWI from the extrapolation of the penetration curve using a numerical fit.

3. Results and discussion

3.1. Vapor spray in nozzle-wall region

In Figure 9, the behavior of free vapor penetration for different ambient temperatures and injection pressures is shown, specifically for a random wall configuration (d_w = 50 mm; θ_w = 90°). Gas temperature does not show important effects on vapor tip penetration. These results are congruent with those found in literature [1, 46]. On the other side, injection pressure has a strong effect on spray velocity since the very beginning of the injection event by means of the significant increase of the momentum flux. Furthermore, this effect is shortened when the system works at higher injection pressures. This variation can also be observed in the bottom plots in terms of *R-parameter*, that is shortened with a decrease in rail pressure and not influenced by ambient temperature. Figure 10 depicts the influence of ambient density and fuel on free penetration, in this case for a free-jet configuration. Momentum transfer between the gas and the spray that is produced in the gas entrainment process at higher ambient densities makes spray advancement through the chamber to be slower. From a comparison between left and right sets of images it can be seen how n-dodecane penetration is consistently faster than for diesel. A possible explanation to that comes from spray theory: Many models for free penetration describe an effect of internal flow [45, 35, 47]. Taking Naber et. al as reference [45], it indicates that $S_v \propto C_a^{0.25} \cdot C_v^{0.5} \cdot D_o^{0.5}$. As the injector is made to avoid cavitation, it is expected not to have significant area contractions and then no variation on C_a or D_o. On the other side, C_v increases with Reynolds number (*Re*), which is inversely proportional to fuel viscosity. nC12 being less viscous than D2 results into a higher C_v, and then a faster penetration. Finally, *R-parameter* of spray penetration is in the bottom set of plots of both Figures 9 and 10, reflecting that, as expected it is nearly constant in the steady part of the spray and also its behavior its in accordance to be proportional to spray momentum. It is important to highlight that the decrease observed near to the wall for some of the curves is produced by the spray reaching the optical limit since it is nearly as dark in the images as the wall and the density gradients in its vicinities.

Some τ_w results that were obtained from spray penetration curves are shown in Figure 11, particularly for different operating conditions. As expected, SWI starts before for low gas densities and high rail pressures, such as gas temperature has no effect on τ_w. Also, the larger the distance between the injector tip and the wall, the longer the time (ASOI) the spray needs to reach the wall. Both reductions of τ_w with d_w and ρ_{amb} seem to be progressively reduced at high rail pressures.

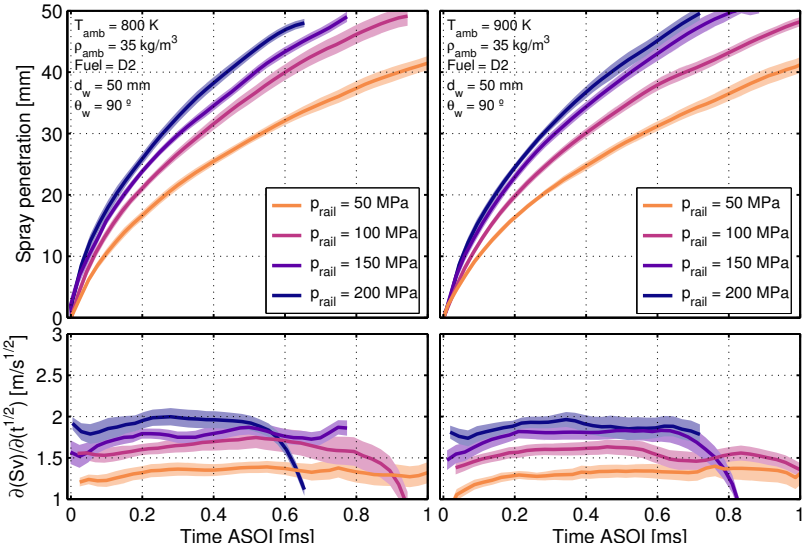

Figure 9: Free vapor penetrations (top) and their *R-parameter* (bottom) for different injection pressures and ambient temperatures (ρ_{amb} = 35 kg m^{-3}; d_w = 50 mm; θ_w = 90°; Fuel = D2). Left: Test conditions at T_{amb} = 800 K. Right: Gas temperature T_{amb} = 900 K

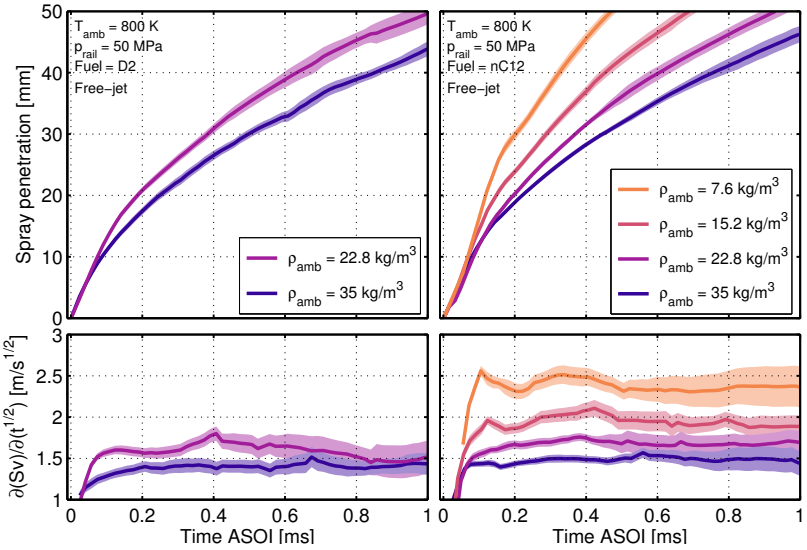

Figure 10: Free vapor penetrations (top) and their *R-parameter* (bottom) for different ambient densities and fuels (T_{amb} = 800 K; p_{rail} = 50 MPa; free-jet). Left: penetrations with diesel #2. Right: Results with n-dodecane

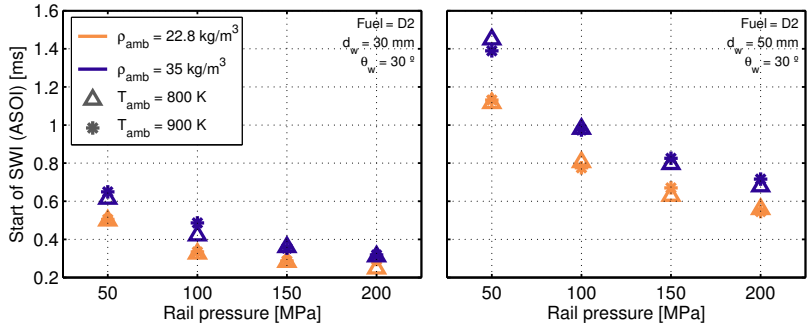

Figure 11: Start of spray-wall interaction calculated for different injection pressures and ambient conditions (θ_w = 30°; Fuel = D2). Left: τ_w at d_w = 30 mm. Right: Results for d_w = 50 mm

The influence of wall conditions and fuel properties on τ_w, are shown in Figure 12. For a fixed d_w, wall angle has not relevant effects on τ_w. On the other hand, there is a noticeable influence of the used fuel that is based on the previously mentioned effect of viscosity, which is weaker than the rail pressure and gas density ones. This effect and even the one of the wall distance, also seem to be less significant as injection pressure is increased.

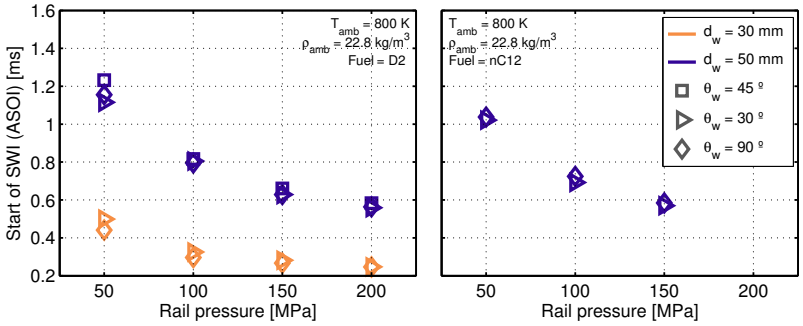

Figure 12: Start of spray-wall interaction calculated for different injection pressures and wall conditions (T_{amb} = 800 K; ρ_{amb} = 22.8 kg m^{-3}). Left: Results for diesel #2. Right: SWI delay for n-dodecane.

3.2. Spray angle

Figure 13 compares vapor spray angle at different ambient densities and temperatures. A higher gas density promotes a higher gas entrainment rate and widens the spray angle. Ambient temperature apparently has no effect on spray angle which is in accordance with literature [48, 45, 49], since both fuels are low viscosity fluids with $(\rho_f/\rho_{amb}) \cdot (Re_f/We_f)^2 > 1$ (this result is higher than 8 for all test points). Additionally, from the comparison between both plots it is seen how the influence of gas temperature and density are equivalent for both free-jet and SWI conditions.

The computed angle results into a steady signal with low fluctuation and uncertainty, which allows to average the values into a windows between 1 ms and 4 ms to obtain a mean spray angle, results that are shown in Figure 14. In this figure, in the left, it can be observed the behavior of spray angle for different operating conditions and fuels, agreeing with density as the strongest factor on widening the angle. No significant effect is observed in rail pressure and a narrowing of the angle is seen for diesel #2 due to its higher viscosity and density ratio (ρ_{amb}/ρ_f) respect to dodecane.

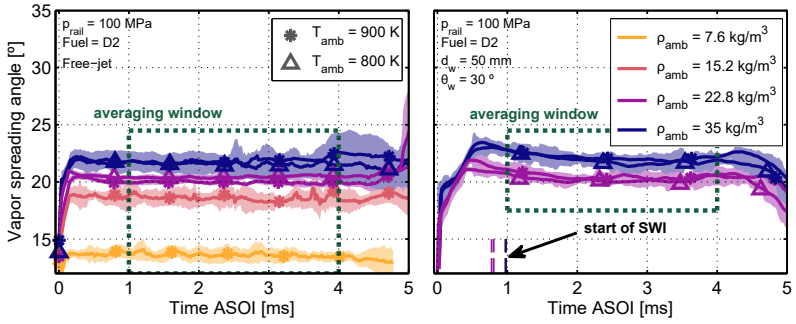

Figure 13: Spray angle vs. time ASOI at different ambient densities and temperatures (p_{rail} = 100 MPa; Fuel = D2). Left: Results for the free-jet configuration. Right: Wall arrangement (d_w = 50 mm; θ_w = 30°)

In Figure 14-right, it can be noted how the wall position has no apparent effect on spray angle. However, and even while it is still within the experimental uncertainty, free-jet angles (green) are consistently narrower than those observed for tests with SWI. This behavior is also in agreement with the contours that are shown in Figure 15, where the impinging sprays have slightly wider angles than the case without a wall. This behavior can be explained in a large extent by the effect of the wall on the gas entrainment. Before collision, both sprays have a similar angle and after SWI starts, the impinging spray is spread in all directions, affecting the spray morphology and leaving part of the spray surface in contact with the wall. Nevertheless, once the spray spreads

more along the wall, the surface in contact with the surrounding gases increases in a greater rate than the free-jet case, allowing more gas entrainment into the spray and widening the angle.

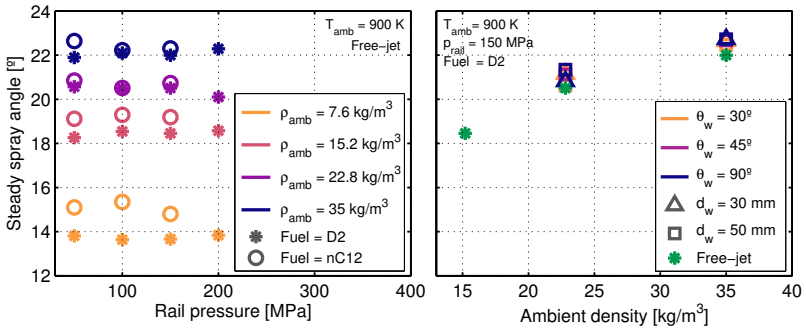

Figure 14: Mean spray angle of different test points. Left: Angle variation with gas thermodynamic conditions, injection pressures and fuels (T_{amb} =900 K; free-jet). Right: Effect of wall configuration (T_{amb} =900 K; p_{rail} = 100 MPa; Fuel = D2)

This increase on surface area that is in contact with the gases, is observed in Figure 16. It has been estimated for ideally axisymmetric sprays (condition nearly seen in free-jet and SWI situations at θ_w = 90°) by the use of Pappus theorem to obtain the surface area of a revolution solid, employing the contour curves in the two halves of the spray, revolving each one π radians. In the cases with a wall, the area in contact with it is found and subtracted from the total area to get the surface that is in contact with the surrounding gas and that is susceptible of contributing to gas entrainment. This gas-spray contact area is plotted in Figure 16 for two different conditions, and it can be observed that its growth rate is similar after SOI, but once SWI is well established, it becomes larger for impinging sprays. While the area for the free-jet constantly increments until the spray reaches the optical limit for SWI cases, the growth rate of spray-gas contact area is faster and it is gradually incremented, what leads SWI to promote gas entrainment and enlarge spray angle. This is better observed in the right graph since free-jet takes more to reach the optical limit due to a lower injection pressure respect to the left plot. It is important to highlight that spray surface calculation is underestimating the antisymmetric-spray surface area since the very thickness of the spray front vortex is covering the real profile of a transversal cut, but this effect is similar for all points and the calculation is still clarifying and qualitatively valid.

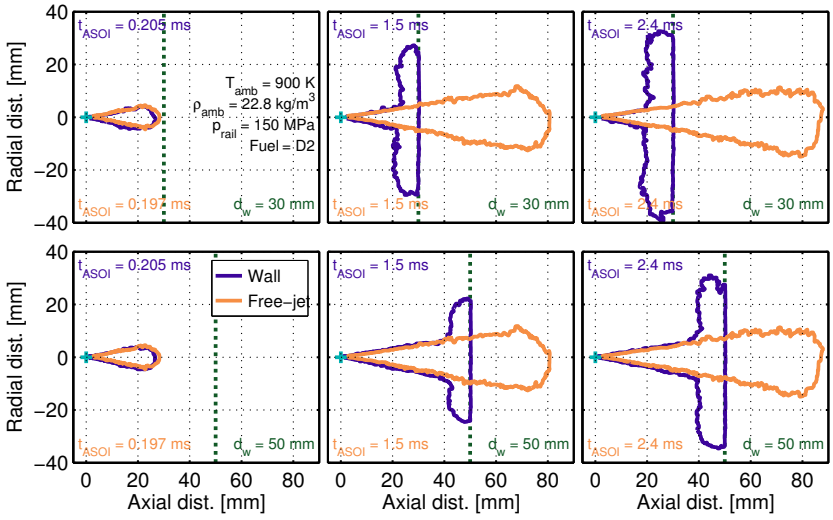

Figure 15: Comparison between SWI and free-jet contours at different times (T_{amb} =900 K; free-jet). Right: Effect of wall configuration (T_{amb} = 900 K; ρ_{amb} = 35 kg m^{-3}; p_{rail} = 150 MPa; Fuel = D2). Top set: Free-jet vs. 30 mm - 90° wall. Bottom set: Free-jet vs. 50 mm - 90° wall

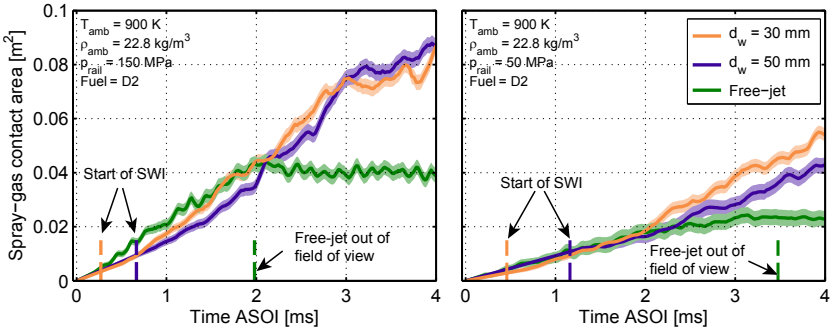

Figure 16: Estimated surface area of the spray that is exposed to the in-chamber gas, compared for ideally axisymmetric sprays (free-jet and sprays against $\theta_w = 90°$ walls). Left: $p_{rail} = 150\,\mathrm{MPa}$. Right: $p_{rail} = 50\,\mathrm{MPa}$

3.3. Vapor SWI visualization

Figures 17; 18 and 19 show spray spreading in the same direction of wall (upwards) vs. time after SWI or τ_w. This temporal reference is useful to achieve a better understanding of the spray-wall interaction from its beginning, helping to have a direct comparison between different conditions. However, from the whole injection perspective, it is also interesting to take into account that the parametrical changes that affect τ_w, will have a different behavior under ASOI reference. For instance, piston geometry or SWI timing could be evaluated by studying atomization and gas-fuel mixing may vary in synchronized injections.

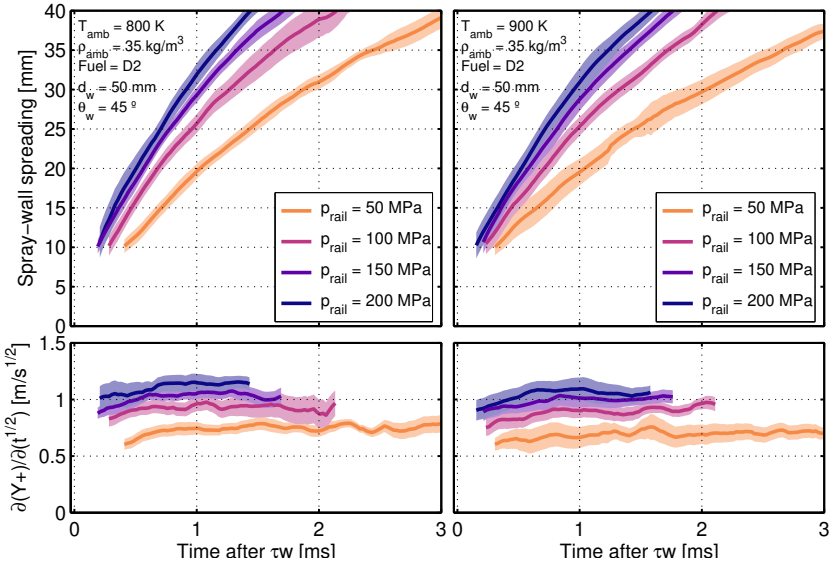

Figure 17: Spreading along the wall (top) and its *R-parameter* (bottom) for different injection pressures and temperatures ($\rho_{amb} = 35\,\mathrm{kg\,m^{-3}}$; $d_w = 50\,\mathrm{mm}$; $\theta_w = 45°$; Fuel = D2). Left: Test conditions at $T_{amb} = 800\,\mathrm{K}$. Right: Gas temperature $T_{amb} = 900\,\mathrm{K}$

Figure 17 shows spray spreading and its respective *R-parameters*, for different rail pressures and ambient temperatures. The trends of those parameters remain the same as previously seen for penetration and, additionally, R_Y is nearly constant as it was observed for R_S. Therefore, spreading is proportional to the square root of time, which establishes a direct analogy between it and free penetration. In other words, even if SWI leads to spray deposition, momentum losses and its distribution in all directions along the wall, the plate does not affect the nature of the spray advancement in a pressurized ambient. However, the values observed for R_Y are lower than the observed for R_S in Figure 9 (same operating conditions and fuel) due to the momentum distribution along all the wall directions, respect to the free spray that goes, broadly speaking in just one direction.

In Figure 18 the analogy between free-jet and SWI cases in terms of the effect of gas density and fuel is also evident. Gas density, as expected, decelerates spray velocity due to gas entrainment effects. On the other side, D2 sprays are slightly slower than nC12 ones due to the differences on viscosities. However, this effect is weak

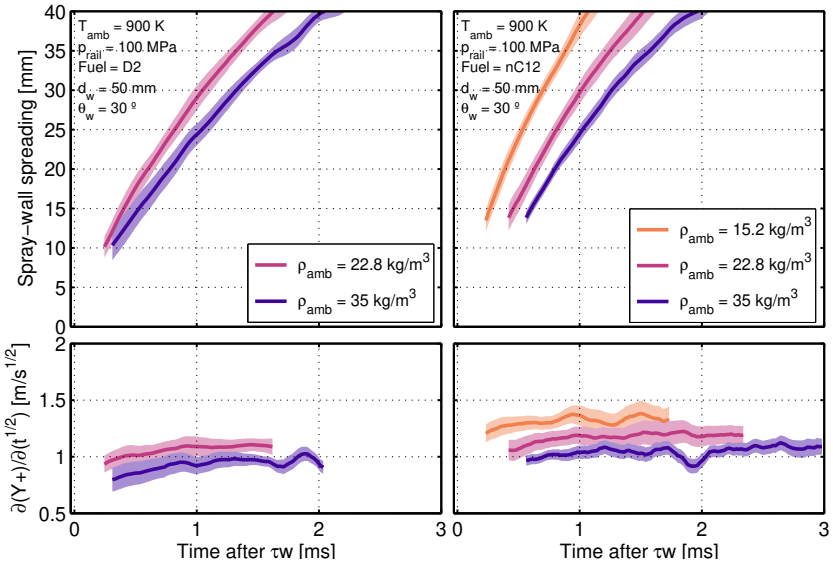

Figure 18: Spreading along the wall (top) and its *R-parameter* (bottom) for different ambient densities and fuels (T_{amb} = 900 K; p_{rail} = 100 MPa; d_w = 50 mm; θ_w = 30°). Left: Spray of diesel #2. Right: Results with n-dodecane

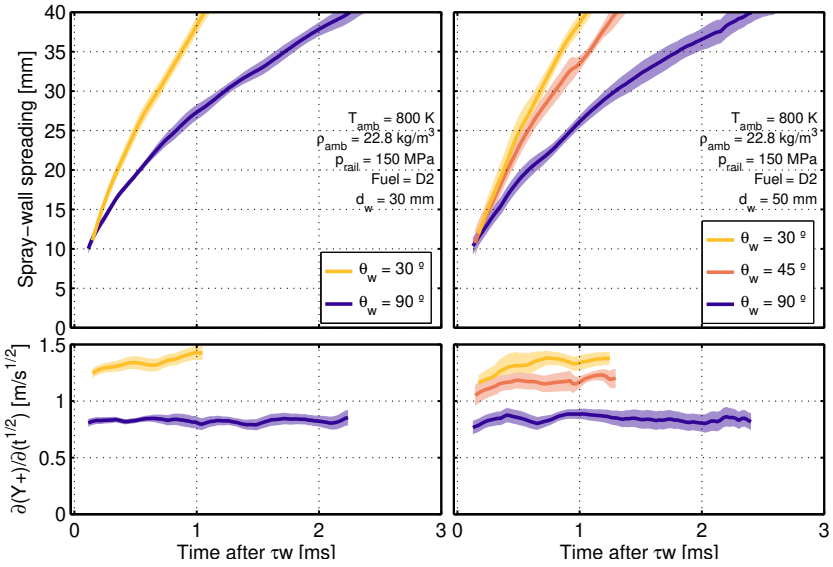

Figure 19: Spreading along the wall (top) and its *R-parameter* (bottom) for different wall positions (T_{amb} = 800 K; ρ_{amb} = 22.8 kg m^{-3}; p_{rail} = 150 MPa; Fuel = D2). Left: Wall at 30 mm from the injector tip. Right: Wall positioned at d_w = 50 mm

in comparison to the one of ambient density.

Finally, regarding wall position, in Figure 19 a comparison of spray spreading for different wall distances and wall angles is shown. What is clear is that narrow wall angles promote a faster spreading due to the heterogeneous distribution of the momentum in all wall directions after impingement. Spray main direction (the one in which Y_+ is measured) suffers less deviation and opposition from the wall and goes faster as it is more similar to be horizontal. In regards to wall distance respect to the injector tip, what it is observed is that in a time reference after τ_w, it has negligible effect in the momentum (visible in *R-parameter*). Not only the effects of a higher impingement velocity and higher losses at a shorter distance are balanced, but momentum flux is similar for both cases. This similarity at different wall distances is observed with a temporal after τ_w reference and it has to be considered that it is strongly affected by wall distance, that is to say, that a spray will spread more on a closer wall for the same time after the start of injection.

An additional value of *R-parameter* definition, is that it does not only allow to characterize spray penetration

in terms of a nearly constant variable (in the steady stage of spray development) that is not dependent of time, but also to establish a direct comparison between free-jet and spray-wall advancement. Figure 20 shows the R_Y/R_S ratio, depicting the proportion of the steady spray-wall spreading respect to free penetration which, due to the redistribution of spray momentum flux in all directions of the wall, is always lower than 1. It is in agreement with the previously shown results how wall distance has no remarkable effect on R_Y/R_S and on the other hand, how wall angle has a very clear control on this momentum distribution that favors the more inclined cases. Nevertheless, it is interesting to highlight how operating conditions (p_{rail} in the X-axis and different ambient temperature and densities in both left and right plots) do not have apparent effect on *R-parameter* ratio, which is to say that the weight of the effect of those parametrical changes is quite similar for both R_S and R_Y. Then, walls that are closer to be horizontal, would exhibit higher R_Y/R_S ratio while results for perpendicular walls converge to 0.4 for the hardware and conditions presented in this work, and to be even more stable with injection pressure, due to the more homogeneous deviation of the spray in all directions of the wall.

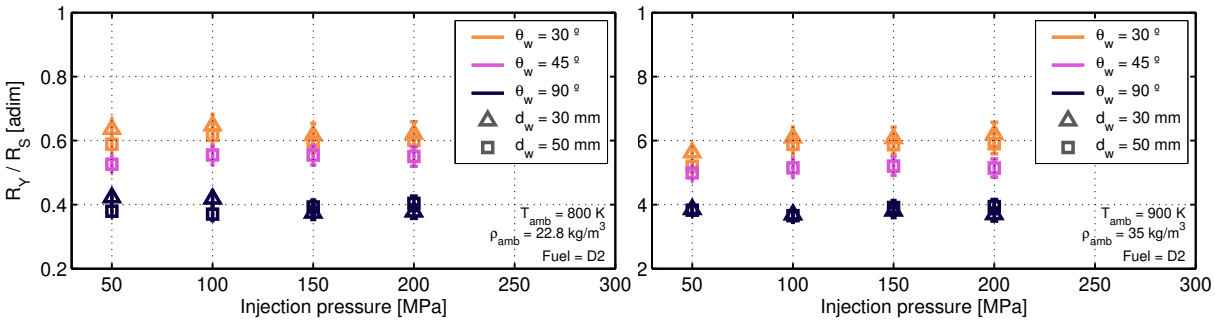

Figure 20: *R-parameter* ratio (R_Y/R_S) for different injection pressures and wall configurations. Left: T_{amb} = 800 K and ρ_{amb} = 22.8 kg m^{-3}. Right: T_{amb} = 900 K and ρ_{amb} = 35 kg m^{-3}.

The results of the spray thickness study are shown in Figures 21, 22 and 23, as mentioned, at 10, 20 and 30 mm from the 'collision point', respectively referred to as Z_{th10}, Z_{th20} and Z_{th30}. First, it can be observed that the pattern that the thickness follows is to present a bump due to the spray head vortex and then to reach a stable value. It is also observed how thickness depends on the measuring point, presenting a thicker spray at larger distances showing how the spray opens as it spreads along the wall. Figure 21 shows thickness for different gas temperature (left) and injection pressure (right). As the other characteristics of the spray, it seems that spray thickness is not affected by ambient temperature. On the other side, in the case of the injection pressure effect,

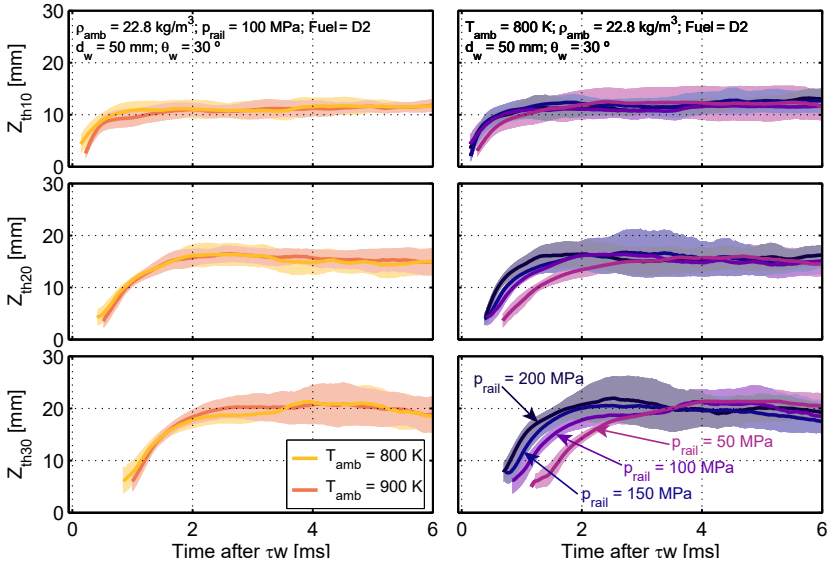

Figure 21: Set of spray thicknesses measured at different wall points varying ambient temperature (left) and injection pressure (right) (ρ_{amb} = 22.8 kg m^{-3}; d_w = 50 mm; θ_w = 30°; Fuel = D2).

it is shown how the peak value is similar for all cases but the stable value is slightly shorter at higher pressures. High rail pressures lead to a faster spray stabilization and shorter spray heights do to its larger spreading component, and the viscous friction inside the spray. The evolution of thickness is also proportional to the square root of time, in accordance with [50].

Regarding the effect of gas density and fuel properties, it is shown in Figure 22. It can be seen how high gas densities promotes thicker sprays due to gas entrainment. The lower density and viscosity of dodecane respect to diesel makes it to be slightly thicker. Additionally, it is also possible to compare the thickness at different measuring points, showing how the spray opens while travels along the wall. From all aforementioned behaviors of spray thickness respect to its profile and how it is affected by different variables, it can be observed that there is a visible analogy between spray angle and spray-wall thickness, as happens between penetration and wall spreading. However, the influence of parametrical variations is slightly weaker for spray thickness due to the partial exposure of an impinging spray to the ambient gas in comparison to a free-jet.

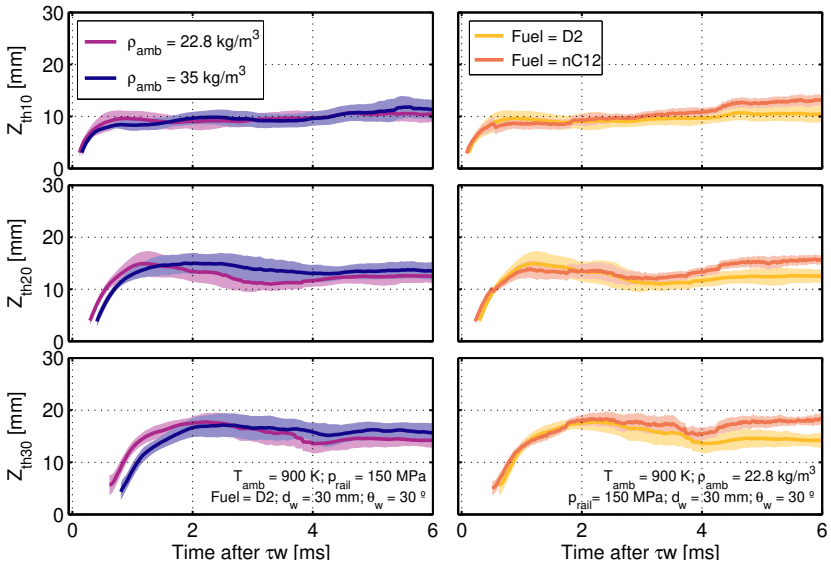

Figure 22: Spray thicknesses for different gas densities (left) and fuels (right) at different distances from the 'collision point' (T_{amb} = 900 K; p_{rail} = 150 MPa; d_w = 30 mm; θ_w = 30°).

Figure 23 shows some tests at different wall positions in terms of distance and inclination. At different wall distances, it can be seen how the stabilization of the thickness is reached quicker and at higher values when the distance is larger. This is produced by two factors: the higher velocity of collision of the spray, which makes the impact and spreading processes more turbulent and initially more unstable, and the shortening on the stage at free-jet conditions. On the other side, the effect of wall angle is also shown, showing a slower stabilization of the thickness at angles closer to perpendicularity, due to the more abrupt deviation of the spray direction and the greater disturbance in the spray morphology. Still, the Z_{th10} plot shows a trend of a developed thicker spray at wider angles, even when the starts of the curves are out of phase due to the variation of spreading velocities with wall angle.

3.4. Free liquid spray visualization

In regards to the liquid phase of the spray that was visualized via DBI, transient liquid penetration is observed in Figure 24-top. As it could be expected, it is largely affected by temperature as a consequence of the enhancement of the kinetic energy of molecules at the spray surface, which reduces the distance that the liquid core is able to reach. Gas density increases gas entrainment rate and improves the mixing rate, shortening liquid penetration too. p_{rail}, on the other side, has negligible effect on liquid length due to the equilibrium between fuel injection rate and gas entrainment increases with rail pressure [51]. Evaporation rate is higher for n-dodecane due to its higher volatility and lower overall distillation temperature, as it is consistently observed in the figure. As an observation, it can be noted how liquid penetration curves are slightly growing in the steady injection stage until reaching a constant value. This has been considered a product of a higher fuel temperature at injection

start because the injector tip is in direct contact with the high temperature gases and then, during the injection event, the fuel flows through the injector and cools the tip down resulting into a larger liquid length. Similarly as happened with the spray angle, an averaging window was taken to calculate a mean liquid length *LL*, in this case, from 2 to 4 milliseconds where the most stable and representative interval is found.

These averaged results are shown in Figure 24-bottom set. The behaviors with parametrical changes remain as mentioned for all the points and show to be significantly weaker at short liquid lengths. Generally it can be said that liquid length is an energy-balance-driven variable while vapor penetration is essentially driven by spray momentum. Dashed lines are used to represent the wall distances of the test plan, and it is seen that there are many points that do not reach any wall and just few of them barely enter in contact with the $50\,\mathrm{mm}$ one, (particularly low temperature and density points) ones. Additionally, through this methodology it was found that the presence of the wall does not affect liquid length when maximum liquid penetration is too short to reach the wall and then, a liquid SWI. Therefore, the set of points for the study of liquid-wall interaction is more limited than for the vapor phase, and the wall at $30\,\mathrm{mm}$ from the injector tip will be the most valuable for information extraction.

3.5. Liquid spray-wall interaction

The influence of changing the wall configuration on liquid spray spreading is illustrated in Figure 25, together with the one of injection pressure. As observed, injection pressure has no important effect on liquid spreading. This leads to an interesting conclusion: this happens not only because the same evaporative mechanisms of liquid length at free-jet conditions apply, but also droplets break-up caused by jet-wall collision does not shorten the liquid spreading by increasing impingement velocity. At free-jet conditions, both fuel injection and gas entrainment rates are incremented and maintain the energy balance, making that liquid length remains unchanged with rail pressure [52, 53]. At SWI conditions, the balance between the droplets break-up given by the impact and the fuel injection rate is also maintained and liquid spreading is mainly driven by evaporation [54, 15]. Regarding wall position, Figure 25-left shows variation on wall distance and it is observed how for the $30\,\mathrm{mm}$ wall, the contact with the spray is well defined while in the $50\,\mathrm{mm}$ it barely reaches the wall. In the right plot, it can be seen how, as it could have been expected from vapor results, the distance that the liquid jet is able to reach is larger if the wall is inclined and has as preferable direction the one in which spreding is measured.

As previously mentioned, spray contour of Schlieren imaging do not represent a transversal cut of the spray due to the gas cloud that is formed by the head front that goes in all directions. This is different for the liquid phase due to the morphology of the colliding jet (Figure 4, bottom) that do not have elements that could cover the central plane of the spray. From this, the assumption of an axisymmetric spray for calculation of variables via

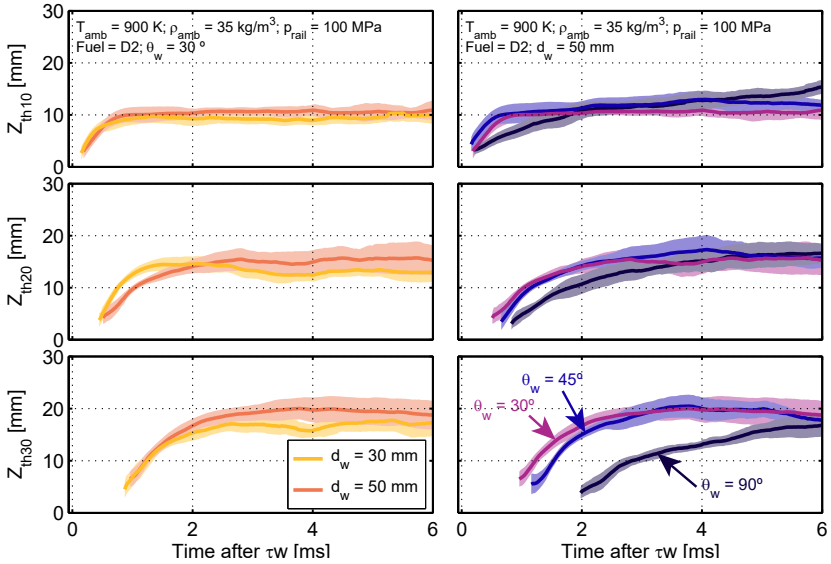

Figure 23: Spray thickness varying wall position. (T_{amb} = 900 K; ρ_{amb} = 35 kg m^{-3}; p_{rail} = 100 MPa; Fuel = D2). Left: Different wall distances from the injector tip. Right: Variation of wall angle respect to nozzle hole axis.

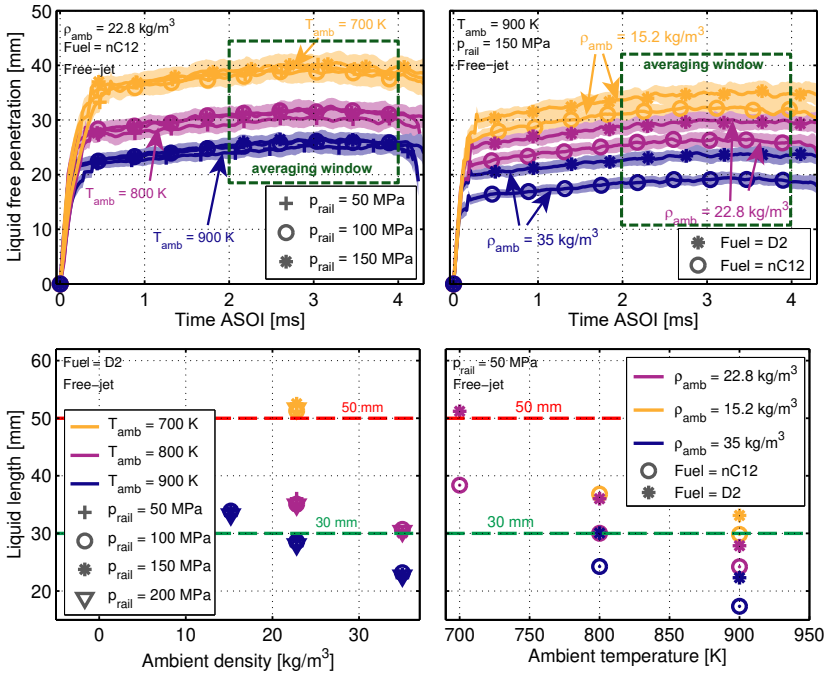

Figure 24: Liquid length at free-jet conditions. Top set: Time resolved liquid penetration at different T_{amb} and p_{rail} (left) and varying fuels and ρ_{amb} (right). Bottom set: Averaged liquid length at a fixed fuel (left) and a single injection pressure (right).

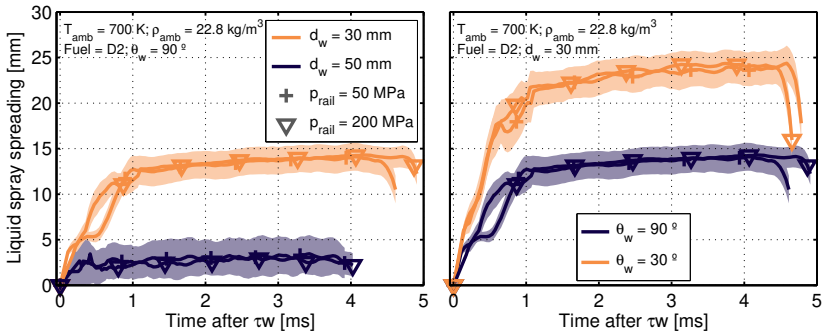

Figure 25: Liquid spray spreading for different wall configurations and injection pressures (T_{amb} = 700 K; ρ_{amb} = 22.8 kg m^{-3}; Fuel = D2). Left: Wall distances comparison. Right: Different wall angles.

Pappus theorem is more accurate for DBI. In this case, the spray volume of the revolution solid has been calculated

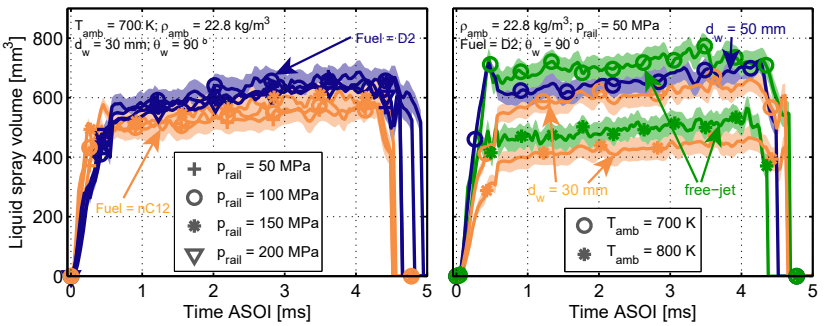

Figure 26: Estimated liquid spray volume for axisymmetric sprays (free-jet and sprays against θ_w = 90° walls). Left: Comparison at different fuels and injection pressures. Right: Varying temperatures of the ambient and wall distance, including free-jet case.

and it is observed for different conditions in Figure 26. This definition is particularly interesting since it allows to compare also points at free-jet conditions in terms of evaporation regime and also because this parameter is independent on how well defined is the jet-wall contact. As it was observed for liquid spreading, the rail pressure effect on spray volume is not important. Evaporation is stronger for n-dodecane than for diesel, which means a shorter steady volume but a larger transitory growth from the start of injection. Ambient temperature has a huge effect con liquid volume as it can be expected from previous results. As spreading, liquid volume is not affected by injection pressure but it is appreciably affected by wall distance. This means that the latter effect can not be attributed to the changes on pre-impingement velocity. An alternative explanation is the prompter change of spray morphology that varies how the exposition to the hot gases is: spray-gas contact area gets larger when the jet impacts in comparison of a free-jet case and this promotes higher gas entrainment and evaporation rates due to the enhancement on heat transfer. This effect is stronger and more significant if the wall is closer to the nozzle outlet, and specially if it is compared to a free-jet case.

3.6. Modeling impinging spray behavior

An accurate prediction of geometrical features of the spray is of great interest for several applications such as design of propulsion systems. A huge amount of correlations have been proposed by different works in order to predict the free-jet [45, 55, 51]. Nevertheless, models for SWI are harder to be found in literature. Different models use a droplet-wall impact to propose correlations for a macroscopic spray development [56, 21]. More sophisticated and complex CFD models are widely used in order to achieve spray simulations at engine-like conditions [48, 57, 58].

This work aims to an intermediate approach, using the large amount data previously gathered (196 test points) to propose some correlations for spray macroscopic behavior at inert conditions. Table 4 indicates the standard form of the models that are proposed in this paper for each parameter and the different parameters that are

Table 4: Summary of the models created for the different parameters obtained from experimental results. Variables inputs and outputs are all in MKS system.

PARAMETER = $\beta_0 \cdot \rho_{amb}^{\beta_1} \cdot \Delta p^{\beta_2} \cdot T_{amb}^{\beta_3} \cdot d_w^{\beta_4} \cdot sin^{\beta_5}(\theta_w) \cdot d_{Zth}^{\beta_6}$

Coefficients	$\boldsymbol{\beta_0}$	$\boldsymbol{\beta_1}$	$\boldsymbol{\beta_2}$	$\boldsymbol{\beta_3}$	$\boldsymbol{\beta_4}$	$\boldsymbol{\beta_5}$	$\boldsymbol{\beta_6}$	$\boldsymbol{R^2}$
Input units	$[-]$	$[\mathrm{kg\,m^{-3}}]$	[Pa]	[K]	[m]	[°]	[m]	[%]
***R-parameter* from spray free penetration $\partial(S_v)/\partial(t^{1/2})$ [m/s$^{1/2}$]**								
D2 (No-wall)	0.03858	-0.245	0.255	0	0	0	0	97.9
nC12 (No-wall)	0.04074	-0.245	0.255	0	0	0	0	98.4
D2 (Any-wall)	0.0390	-0.245	0.255	0	0	0	0	97.4
nC12 (Any-wall)	0.04127	-0.245	0.255	0	0	0	0	97.8
Liquid free length LL [m]								
D2 (No-wall)	26927	-0.4274	0	-1.82	0	0	0	96.4
nC12 (No-wall)	31528	-0.5436	0	-1.812	0	0	0	97.3
Spray vapor angle ϕ_v [°]								
D2 (No-wall)	7.9347	0.2948	0	0	0	0	0	96.1
nC12 (No-wall)	9.4367	0.2478	0	0	0	0	0	96.0
D2 (Any-wall)	8.1220	0.2948	0	0	0	0	0	89.5
nC12 (Any-wall)	9.6537	0.2478	0	0	0	0	0	92.2
Time of start of SWI (ASOI referenced) τ_w [s]								
D2	93.134	0.5025	-0.541	0	-0.125	0	0	99.1
nC12	92.924	0.5025	-0.541	0	-0.125	0	0	98.8
***R-parameter* from spray vapor spreading $\partial(Y_+)/\partial(t^{1/2})$ [m/s$^{1/2}$]**								
D2	0.01602	-0.245	0.255	0	0	-0.6082	0	91.2
nC12	0.01613	-0.245	0.255	0	0	-0.6082	0	89.8
Steady spray thickness along wall Z_{th} [m]								
D2	0.1605	0.16	0	0	0.388	-0.095	0.442	90.1
nC12	0.1675	0.16	0	0	0.388	-0.095	0.442	88.7

included there. Δp is the difference between rail pressure and chamber gas pressure, expressed in Pa and d_{Zth} is the measuring distance of spray thickness along the wall ($10\,\mathrm{mm}$; $20\,\mathrm{mm}$ and $30\,\mathrm{mm}$ as shown in Figures 21; 22 and 23) represented in meters. The equation form has been made generic for all parameters to ease the comparison between different conditions and metrics. In accordance to [51, 46] spray angle is significantly affected by gas density and fuel properties, so the effect shown in the correlations has been implicitly included in the ones of other parameters to keep their standard form, by not expressing them in function of other expressions (i.e. free penetration as function of $tan(\phi_v/2)$ [45, 44]). Additionally, all parameters that remained unchanged for all the test points (such as injector geometrical features, wall material and/or quality-related characteristics, fuel cooling settings, etc) are not expressed in the correlations and are implicitly included into the different coefficients. A similar criterion was used with fuel properties and to difference between free-jet and SWI conditions, that has been to use the coefficient β_0 to absorb those effects. If Table 4 indicates that a coefficient β_i is equal to zero, its parameter is excluded from the correlation for not having statistical significance (high p-value and no important effect on R^2).

As observed before, ambient density and injection pressure are relevant for spray vapor penetration, and the coefficients that are shown in Table 4 in fair match with the proposed by several researchers such as Naber et. al. [45] and Desantes et. al. [44]. The variation between those fuels is slight in agreement with the first results shown in Figure 10 due to their different viscosities. τ_w is, as expected, penetration-like affected. The correlation tailored for liquid length has a high coefficient of determination R^2 with slight variations in β_3, in contrast to β_0 and β_1 as both fuel density and fuel viscosity have an effect on *LL* but the strongest one is given by the evaporative properties of the fuel. Spray spreading on the wall is significantly affected by the impingement angle and spray thickness is considerably sensitive to the measuring point respect to the injector tip and the wall distance respect to the injector nozzle outlet. All these trends and their good agreement with the experimental data is summarized in Figure 27 showing a high confidence degree represented by the narrow area occupied by points around the $x = y$ line, and the generally high R^2 obtained for all the regressions.

4. Conclusions

In the present research, the effect of fuel properties and both operating and wall positioning conditions over the inert spray development in spray-wall interaction situations has been experimentally studied in a constant-flow flow facility. A single-hole ECN injector has been employed in all the experiments to inject two different fuels, and the spray have been observed simultaneously with two cameras using different optical techniques, to visualize its vapor and liquid phases. The geometrical features of the impinging jet has been characterized and some correlations with good agreement with experimental data have been proposed.

Vapor penetration showed to be highly affected by spray momentum flux, while liquid phase variables are driven by vaporization mechanisms that affect heat transfer with the ambient, such as gas density and specially, gas temperature. Spray angle is mainly controlled by gas density by means of gas entrainment. However, the presence of a wall showed an slight widening on spray angle respect to a free-jet due to the change on spray morphology: when the spray starts spreading onto the wall, a larger area of it is exposed to the gases and promotes gas entrainment.

Vapor spreading and vapor free penetration can be considered analogous due to their similar sensitivity to parametrical variations and their proportionality respect to the square root of time. This latter feature made possible the use of a novel variable referred to as *R-parameter* to make an analysis of penetration and spreading regardless of the temporal reference. For inclined walls, the spray has a preferential direction onto the wall and the momentum is not distributed homogeneously in all directions, as ideally happens for a perpendicular wall, which presented a slower spreading in the direction of interest. Another anaglogy was also found between spray angle and spray thickness on the wall, which are similarly affected by the different variables. Furthermore, spray thickness grows as the spray travels further on the wall.

In regards to liquid phase, liquid length showed trends that are in accordance with literature. At SWI conditions, injection pressure showed a negligible influence, and the liquid jet is able to reach larger distances from the collision point with closer and more inclined walls. Liquid jet volume has been calculated and its behavior is similar to the observed for liquid length and spreading. It also allowed to observe that evaporation and air-fuel mixing are not affected by the impinging velocity of the spray, but the change of spray morphology improves its heat transfer with the surrounding hot air.

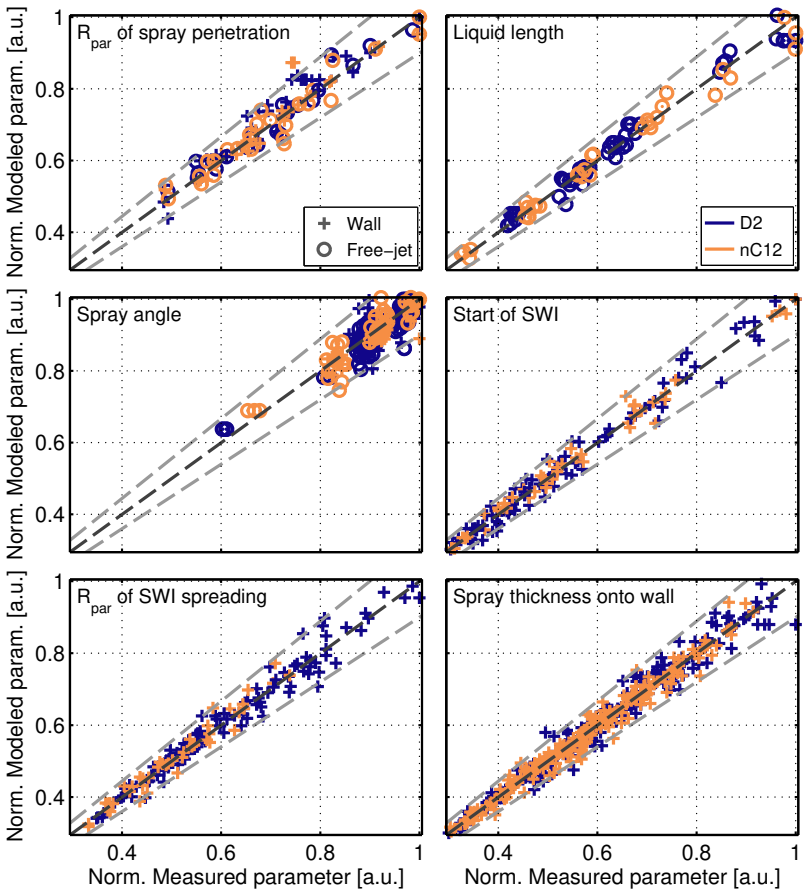

Figure 27: Evaluation of the results from models developed for different variables versus its measured values. The dark gray dashed line represent model = experiment while the lighter lines cover the area of a 10% deviation.

5. Acknowledgments

This research was funded by the Spanish Ministerio de Ciencias, Investigación y Universidades through project reference RTI2018-099706-B-I00. Part of the experimental hardware was purchased through funds obtained from Spanish Ministerio de Ciencia, Innovación y Universidades with FEDER funds through project with reference EQC2018-004605-P.

Finally, the support of Omar Huerta Cornejo and Borja Hurtado in the experiments performance and laboratory work is greatly appreciated.

[1] M. Bardi, R. Payri, L.-M. Malbec, G. Bruneaux, L. M. Pickett, J. Manin, T. Bazyn, C. L. Genzale, Engine Combustion Network: Comparison of Spray Development, Vaporization, and Combustion in Different Combustion Vessels, Atomization and Sprays 22 (2012) 807–842. URL: http://www.dl.begellhouse.com/journals/6a7c7e10642258cc,5b18f0e860ebc687,20adc8ff175d5f43.html. doi:10.1615/AtomizSpr.2013005837.

[2] Y. Jung, J. Manin, S. A. Skeen, L. M. Pickett, Measurement of Liquid and Vapor Penetration of Diesel Sprays with a Variation in Spreading Angle, SAE Technical Paper 2015-01-0946 (2015). doi:10.4271/2015-01-0946.

[3] R. Payri, F. J. Salvador, J. Gimeno, J. E. Peraza, Experimental study of the injection conditions influence over n-dodecane and diesel sprays with two ECN single-hole nozzles. Part II: Reactive atmosphere, Energy Conversion and Management 126 (2016) 1157–1167. URL: http://dx.doi.org/10.1016/j.enconman.2016.07.079. doi:10.1016/j.enconman.2016.07.079.

[4] N. Maes, M. Hooglugt, N. Dam, B. Somers, G. Hardy, On the influence of wall distance and geometry for high-pressure n-dodecane spray flames in a constant-volume chamber, International Journal of Engine Research (2019). doi:10.1177/1468087419875242.

[5] L. Zhao, R. Torelli, X. Zhu, R. Scarcelli, S. Som, H. Schmidt, J. D. Naber, S.-Y. Lee, An Experimental and Numerical Study of Diesel Spray Impingement on a Flat Plate, SAE Int. J. Fuels Lubr. 10 (2017) 407–422. doi:https://doi.org/10.4271/2017-01-0854.

[6] R. Payri, J. Gimeno, J. E. Peraza, T. Bazyn, Spray / wall interaction analysis on an ECN single-hole injector at diesel-like conditions through Schlieren visualization, Proc. 28th ILASS-Europe, Valencia (2017).

[7] C. Tropea, M. Marengo, The Impact of Drops on Walls and Films, Multiphase Science and Technology 11 (1998) 11–36. doi:10.1615/MultScienTechn.v11.i1.20.

[8] S. Y. Lee, S. U. Ryu, Recent progress of spray-wall interaction research, Journal of Mechanical Science and Technology 20 (2006) 1101–1117. doi:10.1007/BF02916010.

[9] A. S. Moita, M. R. O. Panão, Advances and challenges in explaining fuel spray impingement : How much of single droplet impact research is useful ?, Progress in Energy and Combustion Science 36 (2010) 554–580. doi:10.1016/j.pecs.2010.01.002.

[10] M. Panão, A. Moreira, Experimental study of the flow regimes resulting from the impact of an intermittent gasoline spray, Experiments in Fluids 37 (2004) 834–855. doi:10.1007/s00348-004-0868-1.

[11] C. Arcoumanis, P. Cutter, D. S. Whitelaw, Heat Transfer Processes In Diesel Engines, Trans IChemE 76 (1998) 124–132.

[12] U. Meingast, M. Staudt, L. Reichelt, U. Renz, Analysis of Spray / Wall Interaction Under Diesel Engine Conditions, SAE Technical Paper 2000-01-0272 (2000) 1–15.

[13] C. Arcoumanis, P. A. Cutter, Flow and Heat Transfer Characteristics of Impinging Diesel Sprays Under Cross-Flow Conditions, SAE Technical Paper 950448 (1995).

[14] K. Ko, M. Arai, Diesel spray impinging on a flat wall, part i: Characteristics of adhered fuel film in an impingement diesel spray, Atomization and Sprays 12 (2002) 737–751.

[15] M. F. Trujillo, W. S. Mathews, C. F. Lee, J. E. Peters, Modelling and experiment of impingement and atomization of a liquid spray on a wall, International Journal of Engine Research 1 (2000) 87–105. doi:https://doi.org/10.1243/1468087001545281.

[16] R. Rioboo, E. Heat, P. Sa, Outcomes from a Drop Impact on Solid Surfaces, Atomization and Sprays 11 (2001) 155–165. doi:10.1615/AtomizSpr.v11.i2.40.

[17] A. S. Moita, A. L. N. Moreira, Drop impacts onto cold and heated rigid surfaces : Morphological comparisons , disintegration limits and secondary atomization, International Journal of Heat and Fluid Flow 28 (2007) 735–752. doi:10.1016/j.ijheatfluidflow.2006.10.004.

[18] M. Panão, A. Moreira, Thermo- and fluid dynamics characterization of spray cooling with pulsed sprays, Experimental Thermal and Fluid Science 30 (2005) 79–96. doi:10.1016/j.expthermflusci.2005.03.020.

[19] M. Z. Akop, Y. Zama, T. Furuhata, M. Arai, Characteristics of adhesion diesel fuel on an impingement disk wall part 1: Effect of impingement area and inclination angle of disk, Atomization and Sprays 23 (2013) 725–724.

[20] L. Allocca, M. Lazzaro, G. Meccariello, A. Montanaro, Schlieren visualization of a GDI spray impacting on a heated wall: Non-vaporizing and vaporizing evolutions, Energy 108 (2016) 93–98. URL: http://dx.doi.org/10.1016/j.energy.2015.09.107http://linkinghub.elsevier.com/retrieve/pii/S0360544215013171. doi:10.1016/j.energy.2015.09.107.

[21] L. Andreassi, S. Ubertini, L. Allocca, Experimental and numerical analysis of high pressure diesel spray-wall interaction, International Journal of Multiphase Flow 33 (2007) 742–765. URL: http://www.sciencedirect.com/science/article/B6V45-4N0X5XP-1/2/f72e8b50f5fb6f8f324aa18c86883ca8. doi:10.1016/j.ijmultiphaseflow.2007.01.003.

[22] C. Arcoumanis, J. C. Chang, Heat transfer between a heated plate and an impinging transient diesel spray, Experiments in Fluids 16 (1993) 105–119. doi:10.1007/BF00944912.

[23] F. Schulz, W. Samenfink, J. Schmidt, F. Beyrau, Systematic LIF fuel wall film investigation, Fuel 172 (2016) 284–292. URL: http://dx.doi.org/10.1016/j.fuel.2016.01.017. doi:10.1016/j.fuel.2016.01.017.

[24] H. Pan, M. Xu, D. Hung, H. Lv, X. Dong, T. W. Kuo, R. O. Grover, S. E. Parrish, Experimental Investigation of Fuel Film Characteristics of Ethanol Impinging Spray at Ultra-Low Temperature, SAE Technical Paper 2017-01-0851 (2017). doi:https://doi.org/10.4271/2017-01-0851.

[25] H. Zhang, X. Liang, K. Wang, Y. Wang, S. Wang, Experimental study on the interaction between flame propagation and wall film in a confined vessel, Fuel 302 (2021) 121132. URL: https://www.sciencedirect.com/science/article/pii/S0016236121010115. doi:https://doi.org/10.1016/j.fuel.2021.121132.

[26] H. Shi, Q. Tang, Y. An, V. Raman, J. Sim, J. Chang, G. Magnotti, B. Johansson, Study of spray/wall interaction in transition zones from hcci via ppc to ci combustion modes, Fuel 268 (2020) 117341. URL: https://www.sciencedirect.com/science/article/pii/S0016236120303367. doi:https://doi.org/10.1016/j.fuel.2020.117341.

[27] M. Bardi, G. Bruneaux, L.-M. Malbec, Study of ECN Injectors' Behavior Repeatability with Focus on Aging Effect and Soot Fluctuations, SAE Technical Paper 2016-01-0845 (2016). URL: http://papers.sae.org/2016-01-0845/. doi:10.4271/2016-01-0845.

[28] S. A. Skeen, J. Manin, L. M. Pickett, E. Cenker, G. Bruneaux, K. Kondo, T. Aisawa, F. R. Westlye, K. Dalen, A. Ivarsson, X. Tiemin, J. M. García-Oliver, R. D. Reitz, W. Hu, R. D. Reitz, T. Lucchini, G. D. Errico, D. Farrace, S. Pandurangi, Y. M. Wright, M. Chishty, M. Bolla, E. R. Hawkes, A Progress Review on Soot Experiments and Modeling in the Engine Combustion Network (ECN) A Progress Review on Soot Experiments and Modeling in the Engine Combustion Network (ECN) Yuanjiang Pei and Sibendu Som, SAE Int. J. Engines 9 (2016). doi:10.4271/2016-01-0734.

[29] ECN, Engine Combustion Network, Online, 2010. URL: www.sandia.gov/ecn/.

[30] T. D. Fansler, M. F. Trujillo, E. W. Curtis, Spray-wall interactions in direct-injection engines: An introductory overview, International Journal of Engine Research 21 (2020) 241–247. doi:10.1177/1468087419897994.

[31] A. M. Rusly, M. K. Le, S. Kook, E. R. Hawkes, The shortening of lift-off length associated with jet-wall and jet-jet interaction in a small-bore optical diesel engine, Fuel 125 (2014) 1–14. URL: http://dx.doi.org/10.1016/j.fuel.2014.02.004. doi:10.1016/j.fuel.2014.02.004.

[32] C. Fan, D. Wang, K. Nishida, Y. Ogata, Visualization of diesel spray and combustion from lateral side of two-dimensional piston cavity in rapid compression and expansion machine, International Journal of Engine Research (2020) Published online. URL: https://doi.org/10.1177/1468087420962298. doi:10.1177/1468087420962298. arXiv:https://doi.org/10.1177/1468087420962298.

[33] J. E. Peraza, R. Payri, J. Gimeno, P. Martí-Aldaraví, ECN Spray D visualization of the spray interaction with a transparent wall under engine-like conditions. Part II: Impinging spray combustion., Fuel XX (2021) XXX–XXX.

[34] J. Gimeno, P. Martí-Aldaraví, M. Carreres, J. E. Peraza, Effect of the nozzle holder on injected fuel temperature for experimental test rigs and its influence on diesel sprays, International Journal of Engine Research 19 (2018) 374–389. URL: http://journals.sagepub.com/doi/10.1177/1468087417751531. doi:10.1177/1468087417751531.

[35] J. Gimeno, G. Bracho, P. Martí-Aldaraví, J. E. Peraza, Experimental study of the injection conditions influence over n-dodecane and diesel sprays with two ECN single-hole nozzles. Part I: Inert atmosphere, Energy Conversion and Management 126 (2016) 1146–1156. URL: http://dx.doi.org/10.1016/j.enconman.2016.07.077. doi:10.1016/j.enconman.2016.07.077.

[36] R. Payri, F. J. Salvador, J. Manin, A. Viera, Diesel ignition delay and lift-off length through different methodologies using a multi-hole injector, Applied Energy 162 (2016) 541–550. URL: http://linkinghub.elsevier.com/retrieve/pii/S0306261915013549. doi:10.1016/j.apenergy.2015.10.118.

[37] R. Payri, J. Gimeno, J. Cuisano, J. Arco, Hydraulic characterization of diesel engine single-hole injectors, Fuel 180 (2016) 357–366. URL: http://dx.doi.org/10.1016/j.fuel.2016.03.083. doi:10.1016/j.fuel.2016.03.083.

[38] R. Payri, G. Bracho, J. Gimeno, A. Moreno, Spray Characterization of the Urea-Water Solution (UWS) Injected in a Hot Air Stream Analogous to SCR System Operating Conditions, in: WCX SAE World Congress Experience, 2019-01-0738, 2019, pp. 1–9. URL: https://www.sae.org/content/2019-01-0738/. doi:10.4271/2019-01-0738.

[39] L. M. Pickett, C. L. Genzale, J. Manin, L.-M. Malbec, L. Hermant, Measurement Uncertainty of Liquid Penetration in Evaporating Diesel Sprays, in: ILASS Americas 23rd Annual Conference on Liquid Atomization and Spray Systems, ILASS-Americas, Ventura, CA (USA), 2011.

[40] F. R. Westlye, M. Battistoni, S. A. Skeen, J. Manin, L. M. Pickett, A. Ivarsson, Penetration and combustion characterization of cavitating and non-cavitating fuel injectors under diesel engine conditions, SAE Technical Paper 2016-01-0860 (2016) 15. doi:10.4271/2016-01-0860.

[41] F. R. Westlye, K. Penney, A. Ivarsson, L. M. Pickett, J. Manin, S. A. Skeen, Diffuse back-illumination setup for high temporally resolved extinction imaging, Applied Optics 56 (2017) 5028. doi:10.1364/ao.56.005028.

[42] T. Xuan, J. V. Pastor, J. M. García-Oliver, A. García, Z. He, Q. Wang, M. Reyes, In-flame soot quantification of diesel sprays under sooting/non-sooting critical conditions in an optical engine, Applied Thermal Engineering 149 (2019) 1–10. URL: https://doi.org/10.1016/j.applthermaleng.2018.11.112. doi:10.1016/j.applthermaleng.2018.11.112.

[43] R. Payri, J. Gimeno, G. Bracho, D. Vaquerizo, Study of liquid and vapor phase behavior on Diesel sprays for heavy duty engine nozzles, Applied Thermal Engineering 107 (2016) 365–378. doi:10.1016/j.applthermaleng.2016.06.159.

[44] J. M. Desantes, R. Payri, F. J. Salvador, A. Gil, Development and validation of a theoretical model for diesel spray penetration, Fuel 85 (2006) 910–917. URL: http://www.sciencedirect.com/science/article/pii/S0016236105004084.

[45] J. D. Naber, D. L. Siebers, Effects of Gas Density and Vaporization on Penetration and Dispersion of Diesel Sprays, SAE Paper 960034 (1996). doi:10.4271/960034.

[46] R. Payri, F. J. Salvador, J. Gimeno, J. P. Viera, Experimental analysis on the influence of nozzle geometry over the dispersion of liquid n-dodecane sprays, Frontiers in Mechanical Engineering 1 (2015) 1–10. URL: http://journal.frontiersin.org/Article/10.3389/fmech.2015.00013/abstract. doi:10.3389/fmech.2015.00013.

[47] J. S. Giraldo, R. Payri, P. Marti-Aldaravi, T. Montiel, Effect of high injection pressures and ambient gas properties over the macroscopic characteristics of the diesel spray on multi-hole nozzles, Atomization and Sprays 28 (2019) 1145–1160. URL: http://dl.begellhouse.

com/journals/6a7c7e10642258cc,forthcoming,29651.html. doi:10.1615/AtomizSpr.2019029651.

[48] H. Yu, X. Liang, G.-Q. Shu, Y. Wang, H. Zhang, W. Chen, Numerical Investigation of the Effect of Alcohol-Diesel Blending Fuels on the Spray-Wall Impingement Process, SAE Technical Papers 2016-April (2016). doi:10.4271/2016-01-1276.

[49] E. Delacourt, B. Desmet, B. Besson, Characterisation of very high pressure Diesel sprays using digital imaging techniques, Fuel 84 (2005) 859–867. URL: http://www.sciencedirect.com/science/article/pii/S0016236105000062. doi:10.1016/j.fuel.2004.12.003.

[50] Q. Lamiel, N. Lamarque, J. Helie, D. Legendre, On the spreading of high-pressure spray-generated liquid wall films, International Journal of Multiphase Flow 139 (2021) 103619. URL: https://www.sciencedirect.com/science/article/pii/S0301932221000677. doi:https://doi.org/10.1016/j.ijmultiphaseflow.2021.103619.

[51] M. Xu, Y. Cui, K. Deng, One-dimensional model on liquid-phase fuel penetration in diesel sprays, Journal of the Energy Institute 89 (2016) 138–149. URL: http://dx.doi.org/10.1016/j.joei.2015.01.002. doi:10.1016/j.joei.2015.01.002.

[52] D. L. Siebers, Scaling liquid-phase fuel penetration in diesel sprays based on mixing-limited vaporization, SAE Technical Paper 1999-01-0528 (1999). URL: http://subscriptions.sae.org/content/1999-01-0528/. doi:10.4271/1999-01-0528.

[53] D. L. Siebers, Liquid-Phase Fuel Penetration in Diesel Sprays, SAE Technical Paper 980809 (1998) 1–23. URL: http://papers.sae.org/980809/. doi:10.4271/980809.

[54] Y. Zhang, M. Jia, H. Duan, P. Wang, J. Wang, H. Liu, M. Xie, Numerical and experimental study of spray impingement and liquid film separation during the spray/wall interaction at expanding corners, International Journal of Multiphase Flow 107 (2018) 67–81. URL: https://doi.org/10.1016/j.ijmultiphaseflow.2018.05.016. doi:10.1016/j.ijmultiphaseflow.2018.05.016.

[55] J. M. Desantes, R. Payri, F. J. Salvador, J. Gimeno, Prediction of Spray Penetration by Means of Spray Momentum Flux, SAE Technical Paper 2006-01-1387 (2006). doi:10.4271/2006-01-1387.

[56] M. Gavaises, A. Theodorakakos, G. Bergeles, Modeling wall impaction of diesel sprays, International Journal of Heat and Fluid Flow 17 (1996) 130–138. URL: http://www.sciencedirect.com/science/article/pii/0142727X9500097A. doi:http://dx.doi.org/10.1016/0142-727X(95)00097-A.

[57] A. Zhang, A. Montanaro, L. Allocca, J. D. Naber, S.-Y. Lee, Measurement of Diesel Spray Formation and Combustion upon Different Nozzle Geometry using Hybrid Imaging Technique, SAE Technical Paper 2014-01-1410 (2014). URL: http://www.sae.org/technical/papers/2014-01-1410. doi:10.4271/2014-01-1410.

[58] L. Zhao, R. Torelli, X. Zhu, R. Scarcelli, S. Som, H. Schmidt, J. D. Naber, S.-Y. Lee, An Experimental and Numerical Study of Diesel Spray Impingement on a Flat Plate, SAE Int. J. Fuels Lubr. 10 (2017) 407–422. doi:https://doi.org/10.4271/2017-01-0854.